Rayleigh-Bénard convection with two-frequency temperature modulation

Puneet Kaur and Jitender Singh*
Department of Mathematics, Guru Nanak Dev University, Amritsar-143005, Punjab, India

Renu Bajaj†
Department of Mathematics, Panjab University, Chandigarh-160014, India
(Received 27 January 2016; published 12 April 2016)

The response of Rayleigh-Bénard convection in a horizontal fluid layer to time-periodic heating of its horizontal boundaries with a mixture of two frequencies is analyzed numerically. The ratio of the two forcing frequencies and the mixing angle of the amplitudes of modulation provide a control on the instability of the system. In addition to the existence of well-known harmonic and subharmonic instability responses under modulation, the time-periodic oscillation of the boundary temperatures of the fluid-layer with two frequencies results in more bicritical states in comparison to the single-frequency excitation. The onset of instability depends strongly on the modulation parameters and the Prandtl number of the fluid.

DOI: 10.1103/PhysRevE.93.043111

I. INTRODUCTION

Rayleigh-Bénard convection (hereafter referred to as RBC) in a horizontal layer of fluid has become a paradigm among the studies concerning instability phenomena. The study of RBC under different conditions has left a deep imprint on the development of the theory of pattern formation in systems driven away from equilibrium. RBC has great utility in explaining the convection phenomena in diverse areas such as astrophysics, geophysics, engineering, and atmospheric sciences [1,2].

If the fluid layer is parametrically excited by an external time-periodic forcing or the boundary conditions are time-periodic, the instability appears in the form of time-periodic oscillations. The fluid pattern may oscillate either with the forcing frequency or with a frequency that is a submultiple of the forcing frequency. In the former case the oscillations are called harmonic oscillations, whereas in the latter case they are called subharmonic oscillations.

The parametric excitation of the fluid layer via mechanical vibration results in Faraday instability, which was discovered experimentally by Faraday in 1831. For a quick review on Faraday instability, the reader may refer to the work of Miles and Henderson [3].

The time-periodic heating of the boundaries of the horizontal fluid layer results in a time-periodic basic state. The instability of the time-periodic basic state also arises in the form of harmonic or subharmonic oscillations, depending upon the control parameters. This instability is called temperature-modulated Rayleigh-Bénard convection (hereafter referred to as TMRBC) [2,4–12].

Both the Faraday instability as well as TMRBC are well-understood instability phenomena, which have been studied theoretically and observed experimentally for decades. Both share identical harmonic and subharmonic oscillatory patterns, which usually occur in the form of rolls, triangles, squares, and hexagons. These patterns have rotational and translational symmetries.

In Faraday instability and RBC under gravity modulation [13], the quasiperiodic patterns are known to exist near the bicritical state when the two frequency modes with different wave numbers become simultaneously unstable [3,14–18].

Quasiperiodic patterns are those planer patterns that have rotational symmetry but do not possess translational invariance. These patterns oscillate time periodically and are spatially quasiperiodic. They occur due to an interaction between the subharmonic and the harmonic modes of the instability [19,20]. The quasiperiodic patterns are found to occur in hydrodynamics, metallic solids, plane-tiling, liquid crystals, optics, etc., and they are objects of mathematical studies as well [21–23].

Unlike Faraday instability and RBC under gravity modulation, TMRBC has not been explored for the quasiperiodic patterns except in the recent numerical work of Singh *et al.* [24], which focused on the existence of a bicritical state in TMRBC as an intermediate state through which the transition between the critical harmonic and subharmonic responses occurs.

The quasiperiodic patterns in Faraday instability can be easily produced numerically as well as experimentally by generalizing the conventional sinusoidal forcing from one forcing frequency to a mixture of two different forcing frequencies [15,25–27]. Likewise, TMRBC is also expected to exhibit quasiperiodic patterns [24]. So, to analyze TMRBC for such quasicrystalline [28] behavior, it becomes important to generalize the conventional forcing in TMRBC to a mixture of two frequencies, which serves as the objective of our present work. Although Faraday instability and RBC under gravity modulation are well-studied problems for quasiperiodic behavior in hydrodynamics, an exploration of TMRBC for the quasipatterns may be helpful to make a more strict comparison of the theory with the experiments, since TMRBC is free from the mechanical vibrations.

The present research is a continuation of the previous work of the authors on TMRBC [24]. Apart from the search of bicritical states, the present work also aims at a detailed linear instability analysis of the problem for different frequency ratios, and other parameters within the range of experimental verification.

*https://sites.google.com/site/sonumaths2/; sonumaths@gmail.com, puneet.kaur99@gmail.com
†rbajaj@pu.ac.in

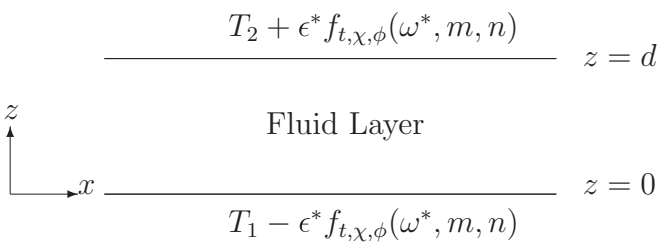

FIG. 1. Diagram showing the time periodically temperature modulated fluid layer confined between the two rigid horizontal planes $z = 0, d$, where f is defined in (1). The fluid layer is assumed to be laterally unbounded.

The paper is planned as follows. Section II describes the problem, where the basic transient state is obtained. In Sec. III, the linear instability analysis of the basic state is done via perturbation analysis supplemented with the Fourier-Floquet analysis, which allows us to search for the periodic states of the instability. The numerical results are presented in Sec. IV. The Prandtl number dependence of the instability is discussed in Sec. V. Finally, the possible conclusions drawn from the numerical results are presented in Sec. VI.

II. THE SYSTEM AND THE BASIC EQUATIONS

We consider a viscous, incompressible, Newtonian fluid, which is also assumed to obey the Boussinesq approximation. The geometrical description of the problem is given in Fig. 1, where the horizontal fluid layer is confined between the two rigid planes $z = 0, d$, $d > 0$.

The temperatures of the horizontal, lower, and upper planes are modulated about their mean values $T_1 > 0$ and $T_2 \geqslant 0$ $(T_2 < T_1)$ in the form $T_1 - \epsilon^* f_{t,\chi,\phi}(\omega^*,m,n)$ and $T_2 + \epsilon^* f_{t,\chi,\phi}(\omega^*,m,n)$, respectively, where

$$f_{t,\chi,\phi}(\omega^*,m,n) = \cos\chi\cos\{m\omega^* t + \phi\} + \sin\chi\cos\{n\omega^* t\}. \tag{1}$$

The symbol $\epsilon^* > 0$ denotes the amplitude of modulation; $\omega_1^* = m\omega^*$ and $\omega_2^* = n\omega^*$, $\omega > 0$ are the two frequencies of modulation, where m and n are coprime positive integers. The parameter $\chi \geqslant 0^\circ$ denotes the mixing angle, which controls the relative amplitudes of modulation corresponding to the two frequencies. For $\chi = 0^\circ$, there is pure ω_1 forcing, and for $\chi = 90^\circ$, there is pure ω_2 forcing. The scalar $\phi \geqslant 0^\circ$ denotes the phase shift between the two forcing frequencies. The phase ϕ lies between 0° and 180°, where $\phi = 0^\circ$ means that ω_1 forcing and ω_2 forcing are in phase.

Let the symbols κ and ρ_0 denote the thermal diffusivity and reference density of the fluid, respectively. To work with the dimensionless quantities, we define the width of the fluid layer d and d^2/κ as the scales for the distance and time, respectively. We use the difference $T_1 - T_2$ to scale the temperature. While making the governing equations [10] dimensionless, we obtain the Rayleigh number Ra, the Prandtl number σ, the modulation amplitude ϵ, and the modulating frequency parameter ω as the dimensionless parameters, which are defined by

$$\mathrm{Ra} = \frac{\alpha d^3 \rho_0 g (T_1 - T_2)}{\kappa\eta}, \quad \sigma = \frac{\eta}{\rho_0\kappa},$$
$$\epsilon = \frac{\epsilon^*}{T_1 - T_2}, \quad \omega = \frac{\omega^* d^2}{\kappa},$$

where g and η in the expression for Ra denote the gravitational acceleration and the coefficient of viscosity of the fluid, respectively. The two dimensionless frequencies of modulation are $\omega_1 = m\omega$ and $\omega_2 = n\omega$, respectively.

The dimensionless system admits the basic state, which can be put in the form $(\mathbf{u}, P, T) = (\mathbf{u}^0, P^0, T^0)$, where the symbols $\mathbf{u}$, P, and T denote the velocity, the pressure, and the temperature of the fluid, respectively, such that

$$\begin{aligned} &\mathbf{u}^0 = \mathbf{0},\ T^0(z,t) = c - z + \epsilon\,\Re\{h(z,t)\}, \\ &P^0 = P(0) + \int_0^z \left[\frac{d^3 g}{\kappa^2} - \sigma\,\mathrm{Ra}(\epsilon\,\Re\{h(z,t)\} - z)\right] dz. \end{aligned} \tag{2}$$

$\Re$ in (2) denotes the real part of the quantity, and $c = \frac{T_1}{T_1 - T_2}$. The modulation of the boundary temperatures results in the unsteady basic state of the system with the appearance of the following function:

$$h(z,t) = \cos\chi\, h_1(z,t) + \sin\chi\, h_2(z,t), \tag{3}$$

where for each $j = 1,2$,

$$h_j(z,t) = \frac{\sinh\{\lambda_j(z-1)\} + \sinh\{\lambda_j z\}}{\sinh\lambda_j} e^{\lambda_j^2 t + \iota(2-j)\phi}, \tag{4}$$

such that $\lambda_j = \sqrt{\iota\omega_j}$. Observe from (2)–(4) that the basic-temperature profile has the following symmetry:

$$T^0(1-z,t) - c + 1/2 = -[T^0(z,t) - c + 1/2]. \tag{5}$$

To study the linear instability response of the basic state (2), we impose infinitesimal perturbation on it in the form

$$\mathbf{u} = \mathbf{u}^0 + (u,v,w),\ T = T^0 + \theta,\ P = P^0 + p, \tag{6}$$

where u, v, w, θ, and p are smooth functions of the space and time variables.

The perturbed state (6) satisfies the equation of continuity and the linearized forms of the Navier-Stokes equations and the energy equation of fluid mechanics, which after simplification reduce to the following linear PDEs:

$$\frac{\partial u}{\partial x} + \frac{\partial v}{\partial y} + \frac{\partial w}{\partial z} = 0, \tag{7a}$$

$$\frac{\partial u}{\partial t} = -\frac{\partial p}{\partial x} + \sigma\left(\frac{\partial^2 u}{\partial x^2} + \frac{\partial^2 u}{\partial y^2} + \frac{\partial^2 u}{\partial z^2}\right), \tag{7b}$$

$$\frac{\partial v}{\partial t} = -\frac{\partial p}{\partial y} + \sigma\left(\frac{\partial^2 v}{\partial x^2} + \frac{\partial^2 v}{\partial y^2} + \frac{\partial^2 v}{\partial z^2}\right), \tag{7c}$$

$$\frac{\partial w}{\partial t} = -\frac{\partial p}{\partial z} + \sigma\left(\frac{\partial^2 w}{\partial x^2} + \frac{\partial^2 w}{\partial y^2} + \frac{\partial^2 w}{\partial z^2}\right) + \sigma\,\mathrm{Ra}\theta, \tag{7d}$$

and

$$\frac{\partial \theta}{\partial t} + w\frac{\partial T^0}{\partial z} = \frac{\partial^2\theta}{\partial x^2} + \frac{\partial^2\theta}{\partial y^2} + \frac{\partial^2\theta}{\partial z^2}, \tag{7e}$$

respectively, where $(x,y,z) \in \Omega = \mathbb{R}^2 \times [0,1]$.

The boundary conditions for the perturbations at the horizontal rigid planes bounding the fluid layer are given by

$$(u,v,w,\theta) = (0,0,0,0) \text{ on } \partial\Omega. \tag{8}$$

III. LINEAR INSTABILITY ANALYSIS

The linear system (7a)–(7e) is homogeneous along the horizontal and is periodic in t. Also, w and θ are bounded on Ω. Therefore, the Fourier-Floquet analysis of the system can be done [10,15,29,30], which we outline here in brief. Eliminating u, v, and p from (7a) to (7e), the resulting system of equations involves only w and θ. Taking into consideration the boundary conditions (8), the perturbations w and θ are expanded in the following Fourier-Floquet form:

$$\begin{pmatrix} w \\ \theta \end{pmatrix} = \sum_{\ell=1}^{N} \sum_{q=-L}^{L} \begin{pmatrix} w_{\ell q}\psi_\ell(z) \\ \sqrt{2}\theta_{\ell q}\sin(\ell\pi z) \end{pmatrix} e^{\iota \mathbf{k}\cdot\mathbf{x}} e^{(s+\iota q\omega)t}, \tag{9}$$

where $\mathbf{k} = (k_1 x, k_2 y)$ and $\mathbf{x} = (x,y)$. The positive integers N and L are chosen large enough in order to meet the numerical convergence. For each ℓ, ψ_ℓ denotes the Chandrasekhar function [1]. The parameter s in (9) is the Floquet exponent. The instability response is *harmonic* for $s = 0$ and *subharmonic* of order $1/2$ for $s = \iota\omega/2$. Using expansions for w and θ from (9) in the aforementioned linear system of PDEs, multiplying throughout by ψ_j and $\sin\{j\pi z\}$ $(1 \leqslant j \leqslant N)$ appropriately, and integrating with respect to z on interval $[0,1]$, we obtain the following set of linear algebraic equations:

$$\begin{aligned}(\mathbf{A}_q - \mathrm{Ra}\mathbf{B})\zeta_q &= \epsilon\cos\chi\{\mathbf{H}_1\zeta_{q-m} + \overline{\mathbf{H}}_1\zeta_{q+m}\} \\ &\quad + \epsilon\sin\chi\{\mathbf{H}_2\zeta_{q-n} + \overline{\mathbf{H}}_2\zeta_{q+n}\}\end{aligned} \tag{10}$$

for each $q = -L, -L+1, \ldots, L-1, L$, where

$$\zeta_q = (w_{1q}w_{2q}\cdots w_{Nq}\theta_{1q}\theta_{2q}\cdots\theta_{Nq})', \tag{11}$$

$$\mathbf{A_q} = \begin{pmatrix} \mathbf{A}^{\mathbf{q}}_{\mathbf{11}} & \mathbf{o} \\ -\mathbf{b}' & \mathbf{A}^{q}_{22} \end{pmatrix}, \quad \mathbf{B} = -k^2\begin{pmatrix} \mathbf{o} & \mathbf{b} \\ \mathbf{o} & \mathbf{o} \end{pmatrix}, \tag{12}$$

such that the matrix $\mathbf{b}$ is defined by

$$\mathbf{b}_{j\ell} = \sqrt{2}\int_0^1 \sin\{\ell\pi z\}\psi_j dz, \quad 1 \leqslant \ell, \quad j \leqslant N. \tag{13a}$$

The entries of the matrices $\mathbf{A}^q_{11}$ and $\mathbf{A}^q_{22}$ are given by

$$\begin{aligned}\left(\mathbf{A}^q_{11}\right)_{j\ell} &= \frac{1}{\sigma}(\mathbf{a}_{j\ell} - k^2\delta_{\ell j})(s + \iota\omega q) \\ &\quad - (k^4 + \mu^4)\delta_{\ell j} + 2k^2\mathbf{a}_{j\ell},\end{aligned} \tag{13b}$$

$$\left(\mathbf{A}^q_{22}\right)_{j\ell} = \{s + \iota\omega q + k^2 + \ell^2\pi^2\}\delta_{j\ell},\ \mathbf{o}_{j\ell} = 0, \tag{13c}$$

where $\delta_{j\ell}$ is the Kronecker delta, and $k = \sqrt{k_1^2 + k_2^2}$ is the wave number of the perturbations. The other coefficients are as follows:

$$\mathbf{a}_{j\ell} = \int_0^1 \psi_j \frac{\partial^2\psi_\ell}{\partial z^2} dz, \tag{13d}$$

and for each $i = 1,2$,

$$\mathbf{H}_i = -\frac{1}{2}\begin{pmatrix} \mathbf{o} & \mathbf{o} \\ (\mathbf{c}^i + \mathbf{d}^i) & \mathbf{o} \end{pmatrix} e^{\iota(2-i)\phi}, \tag{13e}$$

where the matrices $\mathbf{c}^i$ and $\mathbf{d}^i$ are defined by

$$\mathbf{c}^i_{j\ell} = \frac{\sqrt{2}\lambda_i}{\sinh\lambda_i}\int_0^1 \cosh\{\lambda_i(z-1)\}\sin\{\ell\pi z\}\psi_j dz \tag{13f}$$

and

$$\mathbf{d}^i_{j\ell} = \frac{\sqrt{2}\lambda_i}{\sinh\lambda_i}\int_0^1 \cosh\{\lambda_i z\}\sin\{\ell\pi z\}\psi_j dz, \tag{13g}$$

respectively. The overhead bar in $\overline{\mathbf{H}}_i$ in (10) denotes the complex conjugate of $\mathbf{H}_i$. The system (10) can be reduced to an eigenvalue problem of the form

$$SZ = \mathrm{Ra}UZ, \tag{14}$$

where S and U are banded square matrices of order $2N(2L+1)$, and Z is the $2N(2L+1)\times 1$ matrix of the unknown coefficients $w_{\ell q}$ and $\theta_{\ell q}$. The matrix S is nonsingular, and Ra^{-1} is the eigenvalue of the matrix $S^{-1}U$, from which Ra is computed numerically, for a given set of fixed values of the parameters ϵ, ω, m, n, σ, χ, ϕ, and k. The numerical computation of (14) has been done using MATLAB programming to obtain the critical curves.

For the present calculations, we have observed that the method converges for N in the range 5–8 and L in the range 41–80 within a relative error not exceeding 1%, for various values of $\epsilon,\omega,m,n,\sigma,\chi,\phi$, and the range of Ra considered.

IV. RESULTS AND DISCUSSION

The numerical results correspond to the Prandtl number of air, i.e., $\sigma = 0.71$ unless otherwise specified. We have taken the parameter $\epsilon = 1$. With this, the amplitudes of modulation are $\cos\chi$ and $\sin\chi$. We have used $m/n = 1/2$ in most of the numerical calculations. The effect of the frequency ratio has also been observed.

For a set of fixed parametric values of ϵ, ω, m, n, χ, ϕ, σ, and a trial value of k, (14) is solved numerically for Ra. The calculation is repeated for other values of k in the range 2–8. The critical Rayleigh number Ra_c for the onset of instability is defined by

$$\mathrm{Ra}_c = \inf_k\{\mathrm{Ra}(\epsilon,\omega,m,n,\sigma,\chi,\phi,k)\}, \tag{15}$$

where the critical wave number k_c is the value of k at which Ra_c is achieved.

Figure 2 shows the variation of $\sqrt{\mathrm{Ra}_c}$ with the mixing angle $\chi \in [0,90^\circ]$ for the onset of TMRBC for two values of $\phi = 0^\circ$ and 90°. The fixed parametric values are taken as $\sigma = 0.71$, $m/n = 1/2$, and $\epsilon = 1$. The solid (red and black) curves correspond to $\omega = 5$, and the dashed (blue and green) curves correspond to $\omega = 7$. The critical curves for the in-phase modulation ($\phi = 0^\circ$) and the modulation with the phase shift of $\phi = 90^\circ$ in Fig. 2 are explained separately as follows.

A. Case I: $\phi = 0^\circ$

We first explain the curve corresponding to $\omega = 5$ and $\phi = 0^\circ$ of Fig. 2, which consists of alternate harmonic (thicker) and subharmonic (thinner) parts. The point of intersection of the harmonic and subharmonic parts corresponds to a bicritical state. For $\chi = 0^\circ$, only the first frequency $\omega_1 = \omega$ is

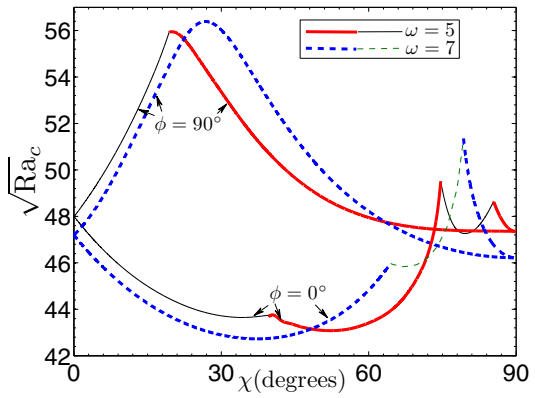

FIG. 2. Critical instability curves in the (χ,Ra$_c$) plane for $\sigma = 0.71$, $m/n = 1/2$, and $\epsilon = 1$. Each of the curves consists of a harmonic (thicker) and a subharmonic (thinner) part. The solid (red and black) and dashed (blue and green) curves correspond to $\omega = 5$ and 7, respectively.

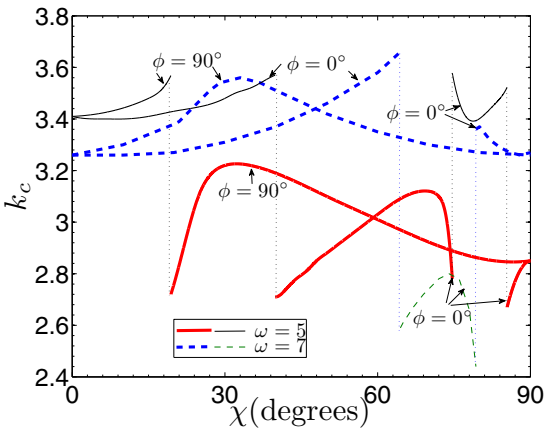

FIG. 3. k_c vs χ for $\sigma = 0.71$, $m/n = 1/2$, and $\epsilon = 1$. The thicker (red and blue) and thinner (black and green) curves correspond to k_c^H and k_c^{SH}, respectively. The solid and dashed curves are drawn for $\omega = 5$ and 7, respectively.

present in the modulation, and the critical instability response is observed to be subharmonic. As χ increases from 0°, the second frequency $\omega_2 = 2\omega$ also contributes to the modulation. For χ small, the dominant frequency is ω_1. Therefore, the terms containing the weaker frequency ω_2 serve as small perturbations in the terms containing the frequency ω_1. Thus, the effect of these perturbations is found to be lower down Ra$_c$. The effect continues with an increase in χ until $\chi \approx 35°$, when the effect of the second frequency ω_2 becomes apparent. With a further increase in χ, Ra$_c$ starts rising. The first bicritical state appears for $\chi \approx 39.87°$, where the critical harmonic and subharmonic wave numbers are $k_c^H = 2.71$ and $k_c^{SH} = 3.58$, respectively, with Ra$_c \approx 1914$. The symbols k_c^H and k_c^{SH} denote the critical wave numbers for the harmonic and subharmonic responses, respectively. On increasing χ beyond 39.87°, the critical instability response is harmonic, and Ra$_c$ also falls down with an increase in χ up to $\chi \approx 52.2°$, where Ra$_c \approx 1857$. Thereafter, a sharp increase in Ra$_c$ with χ is observed up to $\chi \approx 74.66°$, when a second bicritical state occurs. Now the effect of the second frequency ω_2 is dominant, which results in another bicritical state for $\chi \approx 85.422°$. Upon further incrementing χ beyond 85.422°, the critical instability response is harmonic, and Ra$_c$ decreases until $\chi = 90°$. At $\chi = 90°$, only the second frequency ω_2 contributes to the modulation. The details of the bicritical states are given in Table I.

TABLE I. Bicritical states for various values of χ and fixed parametric values of Fig. 2.

ϕ	ω	χ	k_c^H	k_c^{SH}	Ra$_c$
0°	5	39.87°	2.71	3.58	1914.0
		74.66°	2.78	3.58	2451.2
		85.422°	2.67	3.53	2365.8
	7	64.46°	3.66	2.59	2113.3
		79.294°	3.36	2.44	2637.1
90°	5	19.39°	2.72	3.56	3127.9

A similar variation of Ra$_c$ with χ can be observed for $\omega = 7$ and $\phi = 0°$, except that the critical instability response for $\chi = 0°$ and 90° is the harmonic response, and the number of bicritical states is less in comparison to the case $\omega = 5$. The local minima and local maxima on the curve for $\omega = 7$ occur for smaller and higher values of $\sqrt{\mathrm{Ra}_c}$, respectively, if compared to the curve for $\omega = 5$.

B. Case II: $\phi = 90°$

The variation of Ra$_c$ with χ for $\phi = 90°$ in Fig. 2 is different from the case of $\phi = 0°$ for both $\omega = 5$ as well as $\omega = 7$. Here, for $\omega = 5$, the instability response is subharmonic when $\chi = 0°$. The critical value Ra$_c$ increases rapidly with an increase in χ until the bicritical state appears at about $\chi \approx 19.39°$. Beyond the bicritical state, the instability response is harmonic, and Ra$_c$ increases slightly with an increase in χ until a maximum is reached at about $\chi = 20.16°$. Thereafter, Ra$_c$ decreases with a further increase in χ. Similar variation for $\omega = 7$ ($\phi = 90°$) can be observed, but the instability response remains harmonic for all χ. Thus, a 90° phase shift between ω_1 and ω_2 can result in a significant rise of Ra$_c$ in comparison to the in-phase modulation, which is further controlled by the other modulation parameters. However, Fig. 2 suggests that the in-phase modulation should be preferred to produce the bicritical states in TMRBC.

To understand the effect of χ on k_c, Fig. 3 has been obtained in the (χ,k_c) plane for the fixed parametric values as in Fig. 2. The solid and dashed curves are drawn for $\omega = 5$ and 7, respectively. The variation is dramatic, where for $\omega = 5$, $2.67 \leqslant k_c^H \leqslant 3.24$ and $3.40 \leqslant k_c^{SH} \leqslant 3.58$, while for $\omega = 7$, $3.27 \leqslant k_c^H \leqslant 3.68$ and $2.47 \leqslant k_c^{SH} \leqslant 2.80$. Also, observe that $k_c^H < k_c^{SH}$ for $\omega = 5$, and $k_c^H > k_c^{SH}$ for $\omega = 7$ for all χ. These observations together indicate that the harmonic and subharmonic wave numbers for the onset of TMRBC strongly depend upon ω, χ, and ϕ.

For more on the effect of change in the phase shift ϕ between the two modulation frequencies on the onset of TMRBC, we have obtained Fig. 4, which shows the marginal curves in the (k,$\sqrt{\mathrm{Ra}}$) plane for $\sigma = 0.71$, $m/n = 1/2$, $\epsilon = 1$,

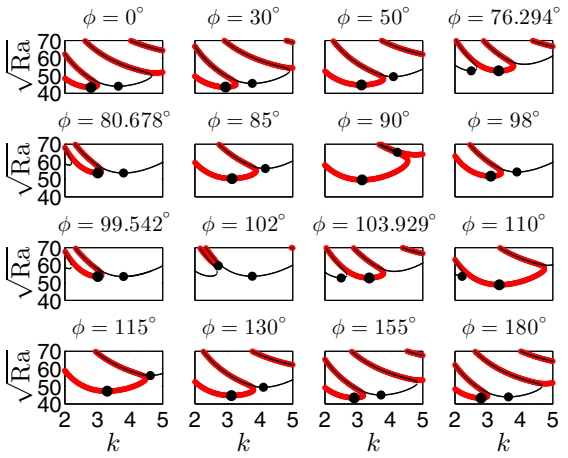

FIG. 4. Instability tongues in the $(k,\sqrt{\mathrm{Ra}})$ plane for $\sigma = 0.71$, $m/n = 1/2, \epsilon = 1$, and $\chi = 45^\circ$. The red (thicker) and black (thinner) parts in each subfigure correspond to harmonic and subharmonic instability responses, respectively. The black mark • corresponds to a local minimum value of $\sqrt{\mathrm{Ra}}$.

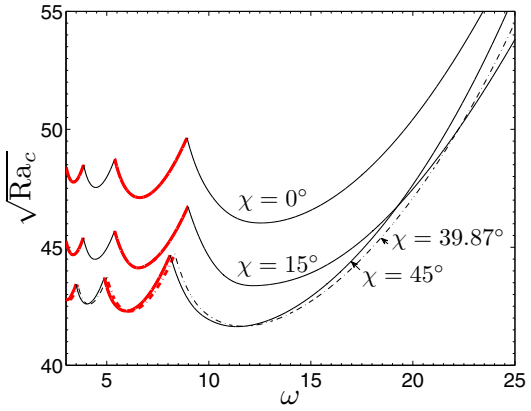

FIG. 5. $\sqrt{\mathrm{Ra}_c}$ vs ω for $\sigma = 0.71, m/n = 1/2, \epsilon = 1$, and $\phi = 0^\circ$. Each of the critical curves consists of a harmonic (red, thicker) and a subharmonic (black, thinner) part.

$\omega = 5$, and $\chi = 45^\circ$. For a fixed ϕ, the marginal-stability curve consists of alternate harmonic red (thicker) and subharmonic black (thinner) parts. The black dot • in each part of the marginal curve corresponds to the minimum value of $\sqrt{\mathrm{Ra}}$. The global minima in each subfigure defines the critical instability response. The first subfigure $\phi = 0^\circ$ represents a state near a bicritical state. With an increase in ϕ, the marginal curves shift toward higher values of $\sqrt{\mathrm{Ra}}$ when a bicritical state appears for $\phi \approx 76.294^\circ$. With a further increase in ϕ, the first two curves of the subfigure $\phi \approx 76.294^\circ$ move upward while the remaining third curve moves downward in the (k,Ra) plane, which results in another bicritical state for $\phi \approx 80.678^\circ$. Upon increasing ϕ beyond 80.678°, the marginal curves move toward the right and downward in the (k,Ra) plane, and the critical instability response remains harmonic up to $\phi = 98^\circ$, when the harmonic and subharmonic curves start moving upward and downward, respectively, resulting in yet another bicritical state for 99.542°. The bicritical states for $\phi = 80.678^\circ$ and 99.542° are approximately the same. Upon increasing ϕ from 99.542°, the harmonic curve moves upward whereas the subharmonic curves move downward in the (k,Ra) plane, where a critical state occurs near $\phi = 102$, with two distinct subharmonic wave numbers. A further movement of the curves upon increasing ϕ results in a bicritical state for $\phi = 103.929^\circ$, which is found to be the same as the one that occurred for $\phi = 76.294$. Upon a further increase in ϕ, the marginal curves move downward in the (k,Ra) plane until $\phi = 180^\circ$. Thus, a change in ϕ may change the nature of instability, the onset of instability, and it may also result in the appearance of bicritical states in TMRBC under two-frequency modulation.

C. Effect of ω

Figure 5 shows the variation of $\sqrt{\mathrm{Ra}_c}$ with ω for different values of χ and fixed values of $\sigma = 0.71$, $m/n = 1/2$, $\epsilon = 1$, and $\phi = 0^\circ$.

For a fixed value of χ, the critical curve is composed of alternate harmonic (red, thicker) and subharmonic (black, thinner) parts. The extent of the harmonic and subharmonic parts increases with an increase in ω, where the increase is significant after $\omega \approx 9$. Also, the alternation of $\sqrt{\mathrm{Ra}_c}$ between harmonic- and subharmonic-type situations can result in advancement or delay in the onset of TMRBC. However, for a fixed value of χ, an increase in ω causes the appearance of bicritical states at a relatively higher Rayleigh number. So, to observe several bicritical states in TMRBC, it will be better to keep ω between 3 and 9. An increase in χ from 0° to 45° shifts the critical curve downward in the $(\omega,\sqrt{\mathrm{Ra}_c})$ plane, which shows an advancement of the onset of the instability. Thus, for the Prandtl number of air, i.e., $\sigma = 0.71$, a mixture of two forcing frequencies has more control on the onset of TMRBC than that of the single forcing frequency.

When the nature of the instability at the onset changes from harmonic to subharmonic for $(\chi,\omega) = (39.87^\circ,3.578)$, $\sqrt{\mathrm{Ra}_c} \approx 43.45$, and k_c changes discontinuously from 3.50 to 2.79. Similarly, when the nature of the instability changes from subharmonic to harmonic for $(\chi,\omega) = (39.87^\circ,5)$, $\sqrt{\mathrm{Ra}_c} \approx 43.75$, and k_c jumps from 2.71 to 3.58. The three bicritical states of Fig. 5 corresponding to $\chi = 39.87^\circ$ occur for $(\omega,\sqrt{\mathrm{Ra}}) \approx (3.578,43.45)$, (5,43.75), and (8.33,44.72) with the wave numbers $(k_c^H,k_c^{SH}) =$ (3.50,2.79), (2.71,3.58), and (3.71,2.56), respectively.

D. Effect of frequency ratio

Figure 6 depicts the variation of $\sqrt{\mathrm{Ra}_c}$ with ω for four values of $m/n = 1/2, 2/3, 4/5$, and $9/10$, and fixed parametric values of $\sigma = 0.71$, $\epsilon = 1$, $\chi = 39.87^\circ$, and $\phi = 0^\circ$. We have taken $\chi = 39.87^\circ$ since it represents a bicritical state for $m/n = 1/2$ and $\omega = 5$. Moreover, the value $\chi = 39.87^\circ$ is near to the value $\chi = 45^\circ$, where both of the modulation frequencies contribute equally. With an increase in m/n from $1/2$ to the other three values in Fig. 6, the bicritical states are observed to appear at comparatively higher values of $\sqrt{\mathrm{Ra}_c}$. For a fixed value of m/n, $\sqrt{\mathrm{Ra}_c}$ can rise or fall, depending upon ω. Note that for $m/n = 1/2$, a high degree of stabilization in TMRBC can be achieved near $\omega = 25$. Also, it seems as if the critical curve tends to shift toward the left in the $(\omega,\sqrt{\mathrm{Ra}_c})$ plane on incrementing m/n. The number of

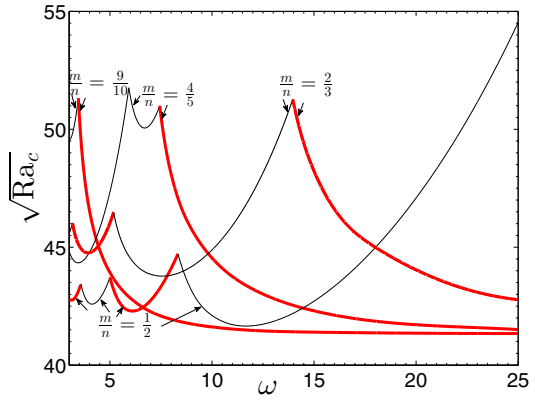

FIG. 6. $\sqrt{\mathrm{Ra}_c}$ vs ω for $\sigma = 0.71, \epsilon = 1, \chi = 39.87^\circ$, and $\phi = 0^\circ$. Each of the critical curves consists of a harmonic (red, thicker) and a subharmonic (black, thinner) part.

bicritical states in the $(\omega, \sqrt{\mathrm{Ra}_c})$ plane also tends to decrease upon increasing m/n. For $m/n = 9/10$, $\mathrm{Ra}_c|_{\omega=25} \approx 1708.8$, which is very close to the value corresponding to the onset of RBC. Thus, for sufficiently large values of ω_1 and ω_2, the harmonic oscillations set in at Ra_c equal to that for the classical RBC.

The critical curve for $m/n = 4/5$ (Fig. 6) is different from the other three curves in the sense that it has two consecutive local minima in the subharmonic segment. Here $(m/n = 4/5)$, as ω is increased from 0, the critical response is subharmonic, and Ra_c increases with ω until $w \approx 5.93$, where $\mathrm{Ra}_c = 2678.8$ with two different values of the critical wave numbers $k_c^{SH} = 2.68$ and 4.02, as is evident from Fig. 7. A further increase in ω favors the onset of the instability by decreasing Ra_c (Fig. 6) until a local minimum is attained at around $\mathrm{Ra}_c = 2505.41$ and $\omega = 6.7$. The critical Rayleigh number again increases with ω until a bicritical state occurs at $\omega \approx 7.44$. Upon increasing ω beyond 7.44, the critical instability response is harmonic, and Ra_c decreases with ω, where $\mathrm{Ra}_c|_{\omega=25} \approx 1722$.

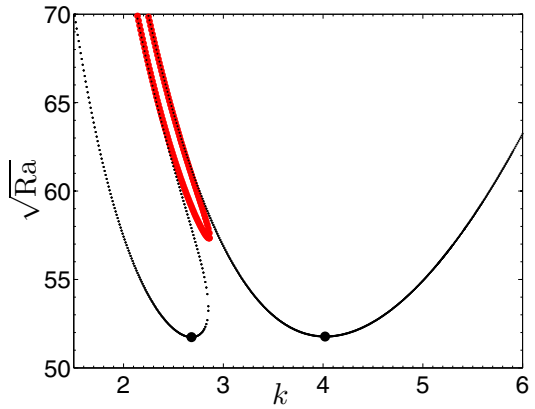

FIG. 7. Instability tongues in the $(k, \sqrt{\mathrm{Ra}})$ plane for $\sigma = 0.71$, $\epsilon = 1$, $\chi = 39.87^\circ$, $\phi = 0^\circ$, $\omega = 5.93$, and $m/n = 4/5$. The red (thicker) and black (thinner) points correspond to harmonic and subharmonic instability responses, respectively. The two black marks • correspond to the overall minimum value of $\sqrt{\mathrm{Ra}}$.

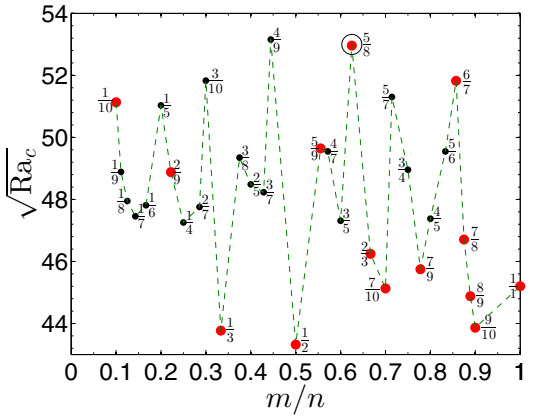

FIG. 8. $\sqrt{\mathrm{Ra}_c}$ vs m/n for $\sigma = 0.71, \epsilon = 1, \omega = 5, \chi = 45^\circ$, and $\phi = 0^\circ$. The larger (red) and smaller (black) points correspond to the harmonic and subharmonic responses, respectively, which are labeled by the corresponding value of m/n. The points are joined by dashed (green) lines in increasing order of m/n. The point marked ○ is for the bicritical state, which is found to occur for $m/n = 5/8$.

To understand the effect of change of m/n on TMRBC for a fixed value of ω, we have obtained Fig. 8, which shows the variation of $\sqrt{\mathrm{Ra}_c}$ with m/n for $\sigma = 0.71$, $\epsilon = 1$, $\omega = 5$, $\chi = 45^\circ$, and $\phi = 0^\circ$. The larger (red) and smaller (black) points correspond to the harmonic and subharmonic responses, respectively, which are labeled by the corresponding frequency ratio $\frac{m}{n}$. The points are joined by dashed (green) lines in increasing order of m/n. It is clear from Fig. 8 that Ra_c may rise or fall in the range 1876–2825 when m/n is varied between 1/10 and 1/1. The onset of instability can be obtained in the form of harmonic or subharmonic oscillations by changing m/n. A bicritical state is also found to occur for $m/n = 5/8$, and it has been marked by ○ in Fig. 8. The variation of Ra_c with m/n for the considered values is sharp, because, with the change of m and n, the values of ω_1 and ω_2 also change simultaneously. We observe that for $\omega = 5$ and $\chi = 45^\circ$, the instability is advanced to the maximum extent for the ratio 1/2, whereas the instability is delayed to the maximum extent for the ratio 4/9.

E. Time profiles

To see the time evolution of the profiles, we have drawn Fig. 9, which shows the variation of $T - T_1/(T_1 - T_2)$ and w with t for the fixed parametric values of $\sigma = 0.71, m/n = 1/2$, $\epsilon = 1$, $\chi = 39.87^\circ$, and $\phi = 0^\circ$. The detail of the curves can be read from the caption of Fig. 9. A homotopic deformation of the basic temperature and vertical-velocity profiles into the profiles corresponding to the bicritical state is evident. At the onset of instability, the temperature profile loses the symmetry of the basic state given by (5), and the vertical velocity is observed to satisfy $w(1 - z, t) \approx w(z, t)$ for all $z \in (0, 1)$ and $t \geqslant 0$.

V. PRANDTL NUMBER DEPENDENCE

The effect of variation of the Prandtl number σ on the onset of TMRBC can be depicted from Fig. 10, which shows the critical instability curve in the $(\sigma, \sqrt{\mathrm{Ra}_c})$ plane for fixed

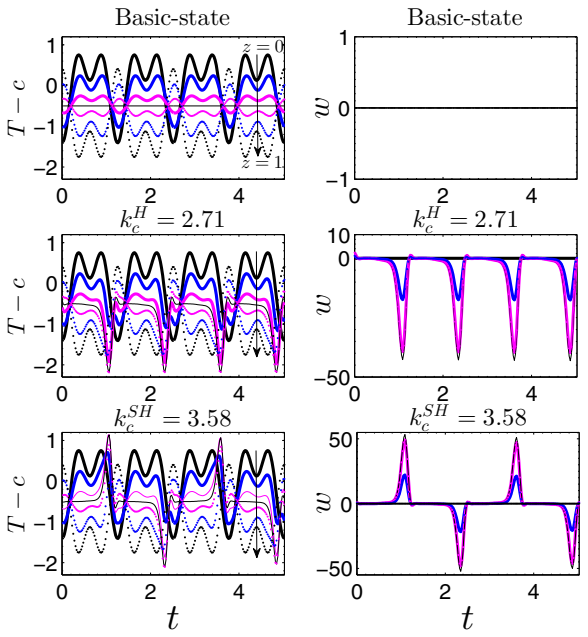

FIG. 9. Time profiles of T-c and w for the bicritical state corresponding to the fixed parametric values of $\sigma = 0.71$, $m/n = 1/2$, $\epsilon = 1$, $\chi = 39.87^\circ$, and $\phi = 0^\circ$. The seven curves in each subfigure correspond to $z = 0$, 0.2, 0.4, 0.5, 0.6, 0.8, and 1, respectively. The arrowhead shows the direction of increase of z. The dotted curves have been drawn for $z = 0.6$, 0.8, and 1 taken in order.

parametric values of $m/n = 1/2$, $\epsilon = 1$, $\omega = 5$, and $\phi = 0^\circ$. The solid (harmonic red and subharmonic black) curves have been drawn for $\chi = 39.87^\circ$, and the dashed (harmonic blue and subharmonic brown) curves correspond to $\chi = 0^\circ$. Here also, for a fixed χ, the critical curve is found to consist of alternate harmonic (thicker) and subharmonic (thinner) parts, which intersect in bicritical states. In each of the two critical

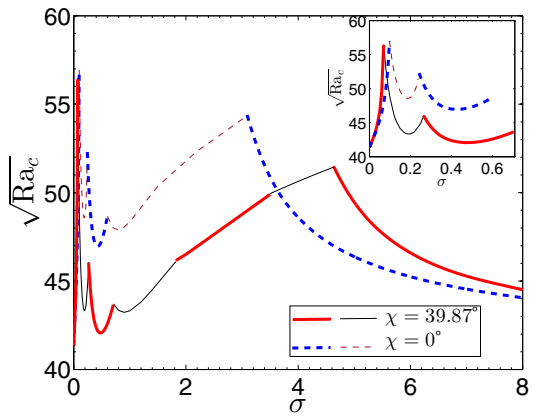

FIG. 10. Variation of $\sqrt{\mathrm{Ra}_c}$ with Prandtl number σ for $m/n = 1/2$, $\epsilon = 1$, $\omega = 5$, and $\phi = 0^\circ$. The thicker and thinner curves correspond to harmonic and subharmonic responses, respectively. The solid and dashed curves have been drawn for $\chi = 39.87^\circ$ and 0°, respectively. For $\chi = 39.87^\circ$, the bicritical states correspond to the fluids with $\sigma \approx 0.0693$, 0.265, 0.71, 1.82, 3.5, and 4.63. For $\chi = 0^\circ$, the bicritical states occur for $\sigma = 0.098$, 0.2425, and 3.09.

TABLE II. Bicritical states for different Prandtl numbers and fixed parametric values of $m/n = 1/2$, $\epsilon = 1$, $\omega = 5$, and $\phi = 0^\circ$.

$\chi = 39.87^\circ$				$\chi = 0^\circ$			
σ	k_c^H	k_c^{SH}	Ra_c	σ	k_c^H	k_c^{SH}	Ra_c
0.0693	4.65	2.87	3186.3	0.098	4.48	2.79	3242.9
0.265	3.50	2.39	2121.0	0.2425	3.42	2.33	2731.0
0.71	2.71	3.58	1914.0	3.09	2.98	3.44	2957.3
1.82	3.61	2.97	2131.0				
3.5	3.58	3.07	2492.3				
4.63	2.23	3.40	2648.8				

curves, for $\sigma = 10^{-4}$, $\mathrm{Ra}_c \approx 1708$, which corresponds to the onset of classical RBC.

We first explain the critical curve corresponding to $\chi = 39.87^\circ$. With an increase in σ beyond 10^{-4}, $\sqrt{\mathrm{Ra}_c}$ rises until $\sigma \approx 0.0693$, where a bicritical state appears. The instability response is subharmonic for $0.0693 < \sigma < 0.265$. The other bicritical states are found to occur for the fluids with Prandtl numbers $\sigma \approx 0.0693$, 0.265, 0.71, 1.82, 3.5, and 4.63, and the details are given in Table II.

Also, for the onset of TMRBC, $\sqrt{\mathrm{Ra}_c}$ can rise or fall with an increase in σ, where $\sqrt{\mathrm{Ra}_c}$ increases almost linearly with σ in the range $1 \leqslant \sigma \leqslant 4.63$, approximately.

For $\chi = 0^\circ$, starting from the value 1708 at $\sigma = 10^{-4}$, Ra_c increases with σ until $\sigma \approx 0.098$ in a manner similar to the case $\chi = 39.87^\circ$. Here, $\sqrt{\mathrm{Ra}_c}$ occurs at a value higher than the value of the one that occurs for $\chi = 39.87^\circ$ in the range $0.098 \leqslant \sigma \leqslant 3.62$. On the other hand, for $\sigma > 3.62$, the onset of instability occurs at a comparatively low value of $\sqrt{\mathrm{Ra}_c}$. In this case, the other bicritical states occur for the fluids with $\sigma = 0.2425$ and 3.09, which have been listed in Table II. Note from this table that the number of bicritical states for the case $\chi = 39.87^\circ$ is more than that of the case $\chi = 0^\circ$.

Finally, we have checked numerically that $\mathrm{Ra}_c|_{\sigma=10^2} \approx 1714$ and $\mathrm{Ra}_c|_{\sigma=10^3} \approx 1708.6$. These observations indicate that

$$\lim_{\sigma\to\infty} \mathrm{Ra}_c = 1708, \tag{16}$$

which is the case of the onset of RBC without modulation. We have further observed numerically that for all χ and ω, the modulation effects are negligible in TMRBC for the fluids of very high and very low Prandtl numbers. Similar variation of $\sqrt{\mathrm{Ra}_c}$ with σ occurs for the other values of χ, ϕ, and m/n, so we have omitted the corresponding calculations. The observations indicate that under modulation, the nature of the onset of TMRBC depends strongly upon the Prandtl number of the fluid under consideration.

VI. CONCLUDING REMARKS

The present work has focused on the investigation of TMRBC in a horizontal fluid layer under time-periodic heating of the two horizontal rigid planes bounding the layer. The time-periodic heating is done via a mixture of two forcing frequencies instead of the single forcing frequency. The linear instability analysis of the underlying dynamical system has been done using the Fourier-Floquet method. Most of the

numerical results are presented for the Prandtl number of air, and the effect of the Prandtl number on the onset of the instability is discussed separately.

With proper tuning of the parameters χ, m/n, ω, and ϕ, the onset of instability in TMRBC can be delayed or advanced as desired. Moreover, the instability may be obtained in the form of harmonic and subharmonic oscillations. Even the bicritical states in TMRBC can be obtained, where the harmonic and the subharmonic oscillations may take place simultaneously.

The critical onset of the instability corresponds to an alternation between the harmonic and the subharmonic responses, which occurs through an intermediate bicritical state, depending upon the modulation parameters. Similar results on the existence of bicritical states have been obtained by Singh *et al.* [24] for TMRBC under single-frequency modulation. However, in the present work, the parameter space for such bicritical states is much wider, i.e., one of the parameters may be varied while fixing the rest of the parameters in order to observe the bicritical states to facilitate experiments on TMRBC. Moreover, for a combination of parameter values such as that for Fig. 7, a critical instability state in TMRBC has been identified, which oscillates with the coexistence of two distinct subharmonic wave numbers.

So, at the onset of TMRBC under two-frequency modulation, the fluid layer may oscillate time periodically with (a) one harmonic wave number or (b) one subharmonic wave number or (c) one harmonic and one subharmonic wave number or (d) two distinct subharmonic wave numbers, depending upon the modulation parameters.

Based on the present numerical calculations, the in-phase modulation in the frequency range 3–8, the mixing angle near 45°, and the frequency ratio of 1/2 are recommendable to excite TMRBC in the air for the bicritical states with a Rayleigh number of about 1900. The modulation effects in TMRBC are significant only for the fluids such as air, which do not have a very high or very low Prandtl number.

TMRBC is expected to exhibit quasiperiodic patterns just like the Faraday problem and RBC under gravity modulation. To observe these patterns explicitly, nonlinear analysis is required. The present numerical work invites experiments on the existence of quasiperiodic patterns in TMRBC near the bicriticality, which is free from mechanical oscillations.

ACKNOWLEDGMENTS

The authors are indebted to the referees for the valuable suggestions and the constructive criticism. P.K. is thankful to the Council of Scientific and Industrial Research (CSIR), New Delhi, India, for providing financial assistance in the form of a Senior Research Fellowship.

[1] S. Chandrasekhar, *Hydrodynamic and Hydromagnetic Stability* (Oxford University Press, Oxford, 1966).
[2] E. L. Koschmieder, *Bénard Cells and Taylor Vortices* (Cambridge University Press, Cambridge, 1993).
[3] J. Miles and D. Henderson, Parametrically forced surface waves, Annu. Rev. Fluid Mech. **22**, 143 (1990).
[4] G. Venezian, Effect of modulation on the onset of thermal convection, J. Fluid Mech. **35**, 243 (1969).
[5] S. H. Davis, The stability of time periodic flows, Annu. Rev. Fluid Mech. **8**, 57 (1976).
[6] C. S. Yih and C. H. Li, Instability of unsteady flows or configurations. Part 2. Convective instability, J. Fluid Mech. **54**, 143 (1972).
[7] G. M. Homsy, Global stability of time-dependent flows. Part 2. Modulated fluid layers, J. Fluid Mech. **62**, 387 (1974).
[8] M. N. Roppo, S. H. Davis, and S. Rosenblat, Bénard convection with time-periodic heating, Phys. Fluids **27**, 796 (1984).
[9] E. Bodenschatz, W. Pesch, and G. Ahlers, Recent developments in Rayleigh-Bénard convection, Annu. Rev. Fluid Mech. **32**, 709 (2000).
[10] J. Singh and R. Bajaj, Temperature modulation in Rayleigh-Bénard convection, ANZIAM J. **50**, 231 (2008).
[11] J. Singh, E. Hines, and D. Iliescu, Global stability results for temperature modulated convection in ferrofluids, Appl. Math. Comp. **219**, 6204 (2013).
[12] J. Singh and S. S. Singh, Instability in temperature modulated rotating Rayleigh-Bénard convection, Fluid Dyn. Res. **46**, 015504 (2014).
[13] U. E. Volmer and H. W. Müller, Quasiperiodic patterns in Rayleigh-Bénard convection under gravity modulation, Phys. Rev. E **56**, 5423 (1997).
[14] W. S. Edwards and S. Fauve, Patterns and quasi-patterns in the Faraday experiment, J. Fluid Mech. **278**, 123 (1994).
[15] T. Besson, W. S. Edward, and L. S. Tuckerman, Two-frequency parametric excitation of surface waves, Phys. Rev. E **54**, 507 (1996).
[16] E. Cerda and E. Tirapegui, Faraday's Instability for Viscous Fluids, Phys. Rev. Lett. **78**, 859 (1997).
[17] C. Wagner, H.-W. Müller, and K. Knorr, Pattern formation at the bicritical point of the Faraday instability, Phys. Rev. E **68**, 066204 (2003).
[18] R. Bajaj, Thermodiffusive magneto convection in ferrofluids with two-frequency gravity modulation, J. Magn. Magn. Mater. **288**, 483 (2005).
[19] D. Binks and W. van de Water, Nonlinear Pattern Formation of Faraday Waves, Phys. Rev. Lett. **78**, 4043 (1997).
[20] D. Binks, M. T. Westra, and W. van de Water, Effect of Depth on the Pattern Formation of Faraday Waves, Phys. Rev. Lett. **79**, 5010 (1997).
[21] D. Shechtman, I. Blech, D. Gratias, and J. W. Cahn, Metallic Phase with Long-Range Orientational Order and No Translational Symmetry, Phys. Rev. Lett. **53**, 1951 (1984).
[22] G. M. Zaslavsky, R. Z. Sagdeev, D. A. Usikov, and A. A. Chernikov, *Weak Chaos and Quasi-regular Patterns* (Cambridge University Press, Cambridge, 1991).
[23] R. Herrero, E. G. Westhoff, A. Aumann, T. Ackemann, Yu. A. Logvin, and W. Lange, Twelvefold Quasiperiodic Patterns in a Nonlinear Optical System with Continuous Rotational Symmetry, Phys. Rev. Lett. **82**, 4627 (1999).
[24] J. Singh, R. Bajaj, and P. Kaur, Bicritical states in temperature-modulated Rayleigh-Bénard convection, Phys. Rev. E **92**, 013005 (2015).

[25] C. Weizhong and W. Rongjue, Instability analysis for Faraday waves under arbitrarily periodic vibration, Sci. China **41**, 1302 (1998).

[26] H. Arbell and J. Fineberg, Pattern formation in two-frequency forced parametric waves, Phys. Rev. E **65**, 036224 (2002).

[27] J. Porter and M. Silber, Broken Symmetries and Pattern Formation in Two-Frequency Forced Faraday Waves, Phys. Rev. Lett. **89**, 084501 (2002).

[28] W. S. Edward and S. Fauve, Parametrically excited quasicrystalline surface waves, Phys. Rev. E **47**, R788(R) (1993).

[29] K. Kumar and L. S. Tuckerman, Parametric instability of the interface between two fluids, J. Fluid Mech. **279**, 49 (1994).

[30] J. Singh and R. Bajaj, Convective instability in a ferrofluid layer with temperature modulated rigid boundaries, Fluid Dyn. Res. **43**, 025502 (2011).